SCIENCE CHINA Materials ARTICLES

mater.scichina.com link.springer.com

Published online 6 September 2018 | 10.1007/s40843-018-9331-x
Sci China Mater 2019, 62(4): 455–464

Enhancing kinetics of Li-S batteries by graphene-like N,S-codoped biochar fabricated in NaCl non-aqueous ionic liquid

Man Huang[1], Jingyu Yang[1], Baojuan Xi[1], Kan Mi[1], Zhenyu Feng[1], Jing Liu[2], Jinkui Feng[3], Yitai Qian[1,4] and Shenglin Xiong[1*]

ABSTRACT **Graphene-like N,S-codoped bio-carbon nanosheets (GNSCS) were prepared by a facile and environment-friendly NaCl non-aqueous ionic liquid route to house sulfur for lithium-sulfur battery. The natural nori powder was calcined at 900°C for 3 h under Ar, in which NaCl non-aqueous ionic liquid can exfoliate carbon aggregates into nanosheets. The structural characterization of GNSCS by a series of techniques demonstrates the graphene-like feature. When evaluated as the matrix for sulfur cathode, GNSCS/S exhibits more prominent cycling stability and rate capability. A discharge capacity of 548 mA h g^{-1} at a current density of 1.6 A g^{-1} after 400 cycles was delivered with a capacity fade rate of only 0.13% per cycle and an initial Coulombic efficiency (CE) as high as 99.7%. When increasing the areal sulfur loading up to 3 mg cm^{-2}, the discharge capacity can still be retained at 647 mA h g^{-1} after more than 100 cycles with a low capacity degradation of only ~0.30% per cycle. The features of N/S dual-doping and the graphene-like structure are propitious to the electron transportation, lithium-ion diffusion and more active sites for chemically adsorbing polysulfides. It is anticipated that other functional biochar carbon can also be attained *via* the low-cost, sustainable and green method.**

Keywords: nori powder, graphene-like N,S-codoped bio-carbon nanosheets, NaCl non-aqueous ionic liquid, reaction kinetics, lithium-sulfur batteries

INTRODUCTION

With the ever-growing demand for energy storage technologies, the advanced battery systems have been intriguing extensive research [1]. Lithium-sulfur (Li-S) batteries have emerged as one of the most attractive candidates to satisfy the next generation commercialized electrochemical power storage sources due to the high theoretical capacity and energy density (1,675 mA h g^{-1} and 2,500 W h kg^{-1}) besides cost effectiveness and environmental friendliness [2]. However, many challenges still should be solved [3]. First, the lower electronic conductivity of sulfur and the discharge products (Li_2S) causes the low utilization of sulfur [4]. Second, the higher solubility of Li_2S_n ($3 \le n \le 8$) in the ether electrolyte leads to a rapid capacity fade and low Coulombic efficiency [5]. Third, the larger volume expansion of about 80% from sulfur to Li_2S is a main reason of the pulverization of the entire electrode [6].

In order to deal with the above problems, specific carbon structures have been selected as hosts for sulfur, including graphite or graphene [7,8], carbon nanotubes/fibers [9,10] and meso/microporous carbon [11,12] and so on [13,14]. However, the synthetic routes developed for these carbon materials have seriously hampered the application of Li-S batteries due to the tedious processing conditions, high cost, and environmental friendliness [15]. For instance, the carbon materials are reported to be derived from different metal-organic frameworks (MOF) precursors [16], which needs hot alkali solution or hydrofluoric acid to remove the metal-involved species. Thus, it is of necessity to search for highly efficient and

[1] Key Laboratory of the Colloid and Interface Chemistry, Ministry of Education, and School of Chemistry and Chemical Engineering, Shandong University, Jinan 250100, China
[2] College of Materials Science and Engineering, Qingdao University of Science and Technology, Qingdao 266042, China
[3] Key Laboratory for Liquid-Solid Structural Evolution & Processing of Materials (Ministry of Education), School of Materials Science and Engineering, Shandong University, Jinan 250061, China
[4] Hefei National Laboratory for Physical Sciences at the Microscale, University of Science and Technology of China, Hefei 230026, China
* Corresponding author (email: chexsl@sdu.edu.cn)

cost-effective sources of carbon to build high performance sulfur-based composites.

The derivation of biochar from biomass has become one of the most popular strategies because the natural materials have intrinsic specialty in terms of structure and composition, let alone the low cost, eco-friendliness and sustainability. To date, various kinds of porous biochar have been reported due to the high yield and easy scalable processes [17,18]. Gu *et al.* [19] explored the microporous carbon material obtained from natural bamboo as the host of sulfur. When the sulfur loading was 50%, the composite showed high initial capacity and Coulombic efficiency (CE). Yu's group [20] reported the preparation of N-doped microporous carbon from human hair and the activation with KOH at 900°C. With the sulfur loading up to 69 wt%, it showed a good reversible capacity of 989 mA h g^{-1} and CE of 99.8% after 300 cycles at 0.2 C. However, in most research documents of biological carbon, the traditional KOH was always used as the activation agent to obtain the targeted carbon materials [20]. But the low yield problem is annoying with respect of the fact that the carbon lost so much after activation. Moreover, the synthesis of graphene-like structure has not been reported based on the biomass source.

Herein, we first proposed a facile and environment-friendly route to prepare graphene-like N/S-codoped biocarbon nanosheets (denoted as GNSCS) by the application of NaCl non-aqueous ionic liquid. As we all know, NaCl is a kind of common ionic crystals. When the temperature is higher than its melting point, i.e., 801°C, NaCl will melt into a non-aqueous ionic liquid [21], which can offer an ionic environment to enhance the diffusivity of starting materials and prevent the agglomeration into the bulk. Cocoon-like β-$CaSiO_3$ nanostructure was reported to be prepared by the solid-state reaction in NaCl–H_2O system [22,23]. Relying on the special functionality of NaCl, we have successfully prepared graphene-like bio-carbon nanosheets by exfoliating the carbon. Moreover, the elements of sulfur and nitrogen from the abundance of amino acids in nori were *in situ* doped into carbon lattice. The as-prepared GNSCS were applied to hold sulfur for Li-S batteries, exhibiting the excellent electrochemical performance even at the condition of high areal sulfur loading.

EXPERIMENTAL SECTION

Materials and chemicals

The nori was purchased from a supermarket and all the other chemicals in our experiments were purchased from Shanghai Sinopharm Chemical Reagent Co. Ltd.

Preparation of GNSCS matrix

The GNSCS was prepared by the carbonization of natural nori. Before using it, the nori was washed with deionized water and ethanol for several times, dried at 80°C overnight, and ground into powder. Then, the mixture of nori powder and NaCl was mixed at a mass ratio of 10:1 with ultrapure water and intensely stirred for 0.5 h, followed by transferring into a 50 mL Teflon-lined autoclave. After sealing, the autoclave was kept at 200°C for 20 h, and then naturally cooled to room temperature. The resulting brown product was heated at 95°C to evaporate water, ground into powder and finally calcined at 900°C under an argon flow with a heating rate of 2°C min^{-1} for 3 h. The product was soaped in 1.0 mol L^{-1} HCl at room temperature for 8 h to remove the impurity to obtain the GNSCS sample.

Preparation of carbon/S composites

In a typical synthesis, the as-obtained powder and sublimed sulfur were mixed with a mass ratio of 2:3 in a glass beaker and then stirred until homogeneous mixing. The obtained carbon/S mixture was heated at 155°C for 10 h under inert atmosphere.

Characterization

The characterization of microstructure and morphology for the as-obtained samples was carried out by field emission scanning electron microscopy (FESEM, G300, Zeiss), and transmission electron microscopy (TEM, JEM-1011 and JEOL-2011). The Bruker D8 X-ray diffractometer with Cu Kα radiation (λ=1.5418 Å) was used to record X-ray powder diffraction (XRD) patterns. The nitrogen adsorption–desorption isotherms were given by Micromeritics ASAP-2020HD88 analyzer at 77 K. The sulfur contents of the composites were tested using MettlerToledoTGA/SDTA851 thermal analyzer from room temperature to 800°C at a heating rate of 5 °C min^{-1} in nitrogen. The X-ray photoelectron spectrum (XPS) was acquired by ESCALAB 250 spectrometer (Perkin-Elmer). The Raman spectra were investigated through NEMUS670 NEXUS670FT-IR Raman spectrometer with an excitation wavelength of 632 nm.

Electrochemical measurements

First, the slurry of the cathode for Li-S batteries, active material, conductive carbon and poly(vinylidenedifluoride) (PVDF) with a ratio of 7:2:1 were dissolved in *N*-methyl-2-pyrrolidinone with stirring for 0.5 h. The

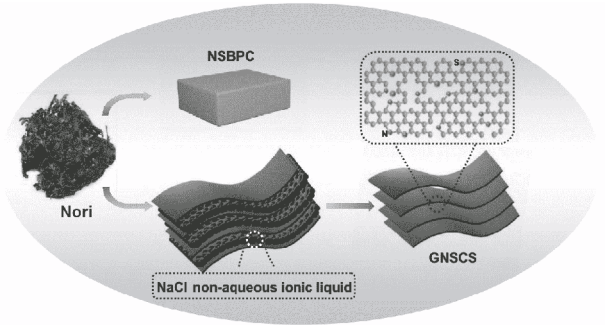

Figure 1 Schematic illustration of the synthesis of graphene-like N,S-codoped bio-carbon nanosheets (GNSCS) and N,S-codoped bulky porous bio-carbon (NSBPC).

slurry was spread onto aluminum foil as the current collector and dried in oven at 60°C for 12 h, which was then cut into disks with a diameter of 12 mm. The 2016R coin-type cells were assembled in an argon-filled glovebox (the value of water and oxygen <0.1 ppm), lithium metal foil worked as the counter electrode, and the separator was Celgard 2400 membrane. The electrolyte was prepared by dissolving 1 mol L^{-1} bis(trifluoromethane) sulfonamide lithium salt (LITFSI, 99%, Acros Organics) in a mixed solvent of 1,2-dimethoxyethane (DME, 99.5%, Alfa Asea), and 1,3-dioxolane (DOL, 99.5%, Alfa Asea) (volumetric ratio of 1:1) with 2 wt% $LiNO_3$ added. The LAND CT2001A charge-discharge testing system was used to test charge–discharge performance at 30°C at a voltage window between 1.7 and 2.8 V *vs.* Li^+/Li. The cyclic voltammetry (CV) at a scan rate of 0.1 mV s^{-1}, electrochemical impedance spectroscopy (EIS) spectra were detected by an electrochemical workstation (CHI 760E, Shanghai Chenhua).

RESULTS AND DISCUSSION

Fig. 1 shows the illustration of the preparation process of the GNSCS from biomass. When nori powder was mixed with NaCl bearing a mass ratio of 10:1, followed by the calcination at 900°C for 3 h under Ar atmosphere. During the process, the NaCl salt melted into non-aqueous ionic liquid composed of Na and Cl ions, which could permeate into the structure of carbon material so that it could been exfoliated into nanosheets. The natural nori is rich in the amino acids which could serve as the source of nitrogen and sulfur [24], which were readily doped *in situ* into the carbon lattice.

The morphology and microstructure of GNSCS were monitored by the technique of FESEM and TEM. As shown in Fig. 2a–d, it is clearly to observe the mor-

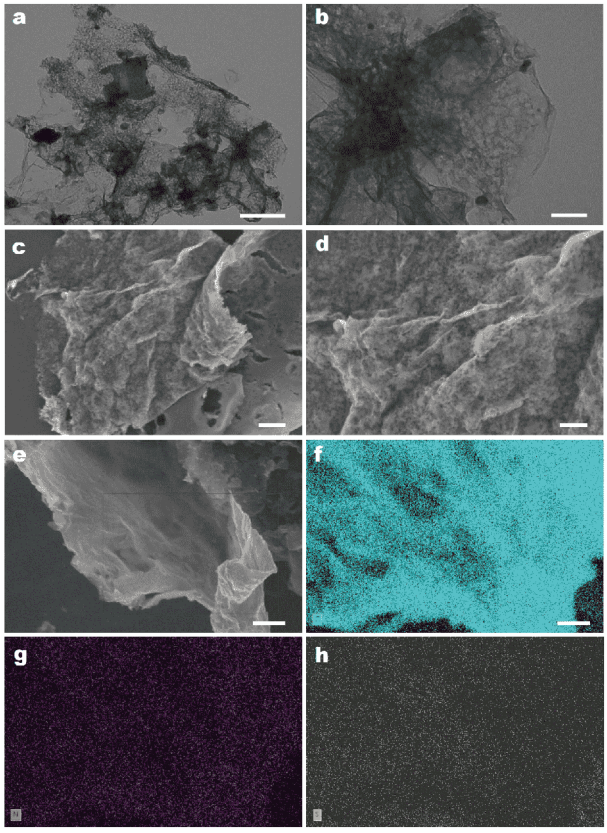

Figure 2 TEM (a, b), FESEM (c, d), and elemental mapping (e–h) images of GNSCSs. Scale bars: (a) 500 nm, (b, d) 100 nm, (c) 200 nm, (e) 250 nm, (f) 150 nm.

phology of graphene-like nanosheets with remarkably porous texture. To demonstrate the role of NaCl non-aqueous ionic liquid in the formation of the nanosheets, a control experiment was conducted by the direct carbonization of the raw natural nori under the same condition except the absence of NaCl to obtain the N,S-codoped bulky porous bio-carbon (denoted as NSBPC). As displayed in Fig. S1, NSBPC consists of bulky aggregates by structure stacking. It can be believed that the formation of graphene-like nanosheets was attributed to the stripping effect of NaCl non-aqueous ionic liquid, which could permeate at higher temperature so that the bulky carbon could be exfoliated into nanosheets. To further explore the elemental component of the GNSCS, the corresponding elemental mappings were measured. Fig. 2e–h shows the homogeneous distribution of carbon, nitrogen and sulfur throughout the GNSCS, which further identifies that N and S are dual-doped into the carbon lattice.

Raman spectra of the two samples are presented in Fig. 3a and both of them have two typical characteristic

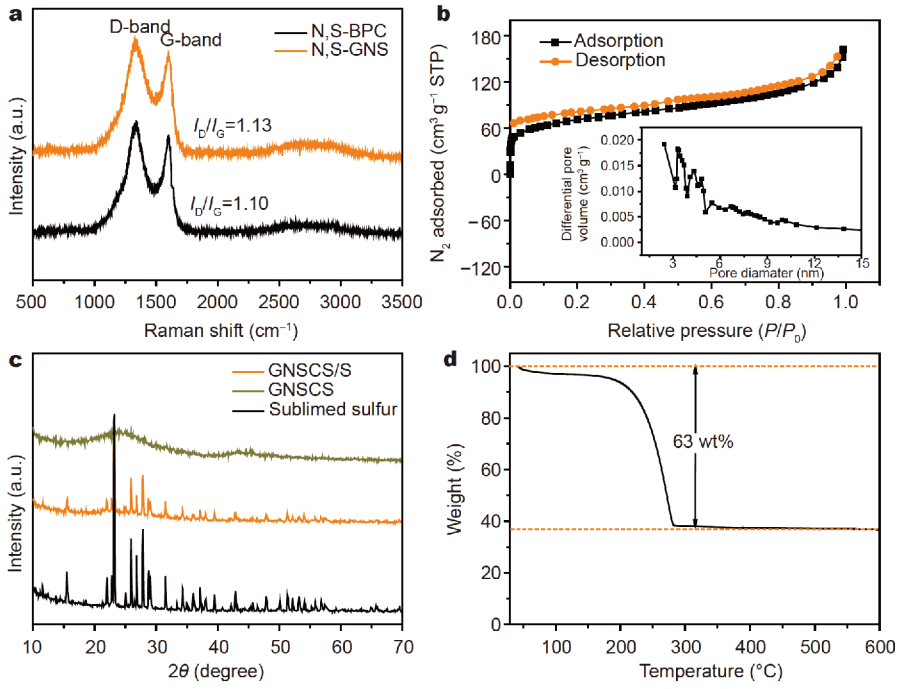

Figure 3 (a) Raman spectra of GNSCS and NSBPC. (b) N_2 adsorption–desorption isotherms and the corresponding pore-size distributions of GNSCS. (c) XRD patterns of pristine sulfur, GNSCS, and GNSCS/S composite. (d) The TGA curve of GNSCS/S sample under inert atmosphere.

peaks, i.e., D band at around 1,348 cm^{-1} and G band at around 1,594 cm^{-1} [25–27]. The former originates from the defective or disordered carbon while the latter is corresponding to the graphitic structure. The ratios of I_D/I_G for GNSCS and NSBPC are 1.13 and 1.10, respectively, resulting from the heteroatoms of N and S doped into the carbon lattice.

The detailed porous texture of GNSCS matrix was investigated by nitrogen adsorption–desorption isotherms. As we can see in Fig. 3b, GNSCS exhibits a type II isotherm (a Langmuir type isotherm). The H4 hysteresis loop is indicative of the slit-like pores present in the GNSCS [28] caused by the sheet structure. The Brunauer–Emmett–Teller (BET) surface area of GNSCS is 249.2 m^2 g^{-1} and the total pore volume is 0.24 cm^3 g^{-1}. From the Barrett-Joyner-Halenda (BJH) pore size distribution curve in the inset of Fig. 3b, mesopores dominate. Hence, the GNSCS are promising for high sulfur loading and could provide more space to accommodate volume expansion [29] (~80%) of sulfur to its discharge production (Li_2S) during the charge–discharge process, and facilitate the lithium ion diffusion.

After combination with sulfur, the composite of GNSCS/S was obtained. The pristine sulfur, GNSCS, and GNSCS/S composite were measured by X-ray diffraction (XRD). As shown in Fig. 3c, two broad peaks at about 25° and 44° are related with the (002) and (101) diffraction peaks of graphitic carbon [30], suggesting a good graphitization degree. What's more, compared with the sharp peaks of pristine sulfur, the peak intensity of the GNSCS/S composite is weaker, corroborating that the part of sulfur particles were successfully distributed in the pores of GNSCS [18,31]. By comparison, XRD patterns of pristine sulfur, NSBPC, and NSBPC/S composite have been shown in Fig. S3c. The sulfur content in the GNSCS/S and NSBPC/S composites is determined to be about 63% by thermogravimetric analysis (TGA) shown in Fig. 3d. The weight loss occurred between 150 and 300°C, ascribed to the evaporation of sulfur in the composite materials.

To further prove the heteroatom doping in GNSCS, the full XPS spectrum is presented in Fig. 4a. The peaks at around 164, 285, 399 and 532 eV are characteristic of S 2p, C 1s, N 1s and O 1s, respectively [32,33]. In addition, the atomic contents of N and S are calculated to be 2.19% and 0.94% in GNSCS. The high-resolution C 1s spectrum in Fig. 4b can be divided into three peaks. The typical peak at 284.7 eV is used as the reference from C–C to calibrate the binding energy of elements. The peaks at 285.6 and 287.4 eV are ascribable to C–S and N–C=O, respectively [24]. As for the S 2p spectrum in Fig. 4c, the notable peaks at 165.2 and 164.0 eV originate from the

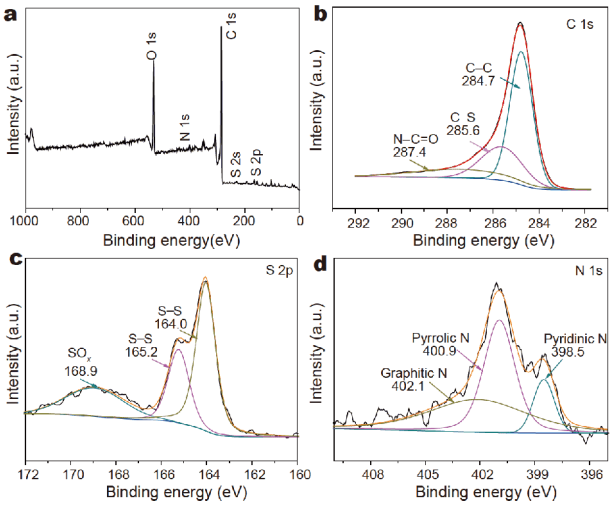

Figure 4 XPS spectra analysis of GNSCS: (a) survey spectrum, (b) C 1s, (c) N 1s, and (d) S 2p.

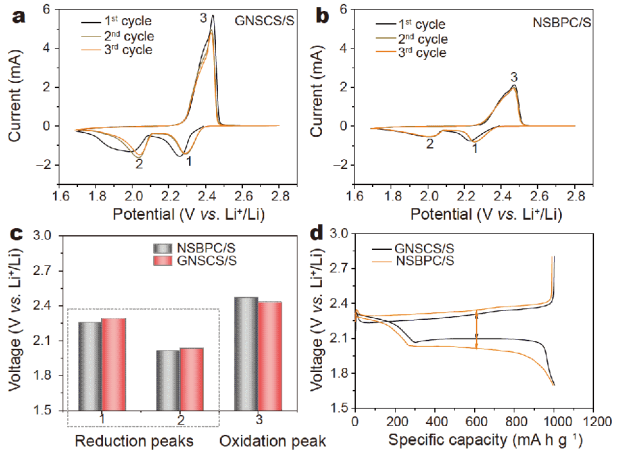

Figure 5 Kinetics of electrochemical reactions in Li-S batteries. (a, b) CV curves and (c) the corresponding peak potentials of 1) GNSCS/S and 2) NSBPC/S electrodes. (d) Charge/discharge voltage profiles of the first cycle at the current density of 300 mA g^{-1}.

signals of S $2p^{1/2}$ and S $2p^{3/2}$ due to their spin orbit coupling. Additionally, the peak at 168.9 eV is featured by the oxidized S (SO_x species) caused by the oxidation of active sulfur in air [34,35]. Three peaks in the N 1s spectrum in Fig. 4d are located at 398.5, 400.9, and 402.3 eV, attributed to pyridinic N, pyrrolic N, and graphitic N, respectively [12,36]. The content of pyridinic N and pyrrolic N can be up to 86.7% which advantageously help raise the electrochemical active sites and anchor the discharge intermediates dissolved in the electrolyte by forming Li_2S_x–N bonding due to the interaction between electrophilic Li^+ and the above electronegative N atoms, effectively inhibiting the dissolution of polysulfides and lithium sulfides and improving the sulfur utilization [37–39]. In addition, the presence of graphitic N was good for increasing electrical conductivity and stability of the carbon framework [40,41] Moreover, S atoms doped in carbon lattice can also confine lithium polysulfides for the reason that S heteroatoms with a lone pair of electrons can serve as electron-rich donors to bond with lithium polysulfides [42]. The above results and analyses all confirm that N and S atoms have embedded in the carbon lattice.

The electrochemical performance of these composites was assessed by assembling coin cells. Fig. 5a, b present the corresponding CV curves scanned at a rate of 0.1 mV s^{-1} within a voltage window between 1.7 and 2.8 V *versus* Li^+/Li. Fig. 5a shows two typical cathodic peaks at 2.29 and 2.04 V in the first scanning, which was attributed to the reduction of S_8 molecules to the higher-order lithium polysulfides and further to Li_2S_2 or Li_2S, respectively [43]. In the anodic curves, two oxidation peaks for the GNSCS/S electrode at 2.38 and 2.48 V are pertaining to the reverse reactions, i.e., the formation of Li_2S_n and further oxidation to sulfur (S_8) [44]. In the following curves, the CV curves are highly overlapped, which indicates the good reversibility of GNSCS/S electrode. The NSBPC/S electrode displayed a similar CV profile in Fig. 5b. However, the redox peaks are widened and much lower in current, indicating a sluggish kinetic process between the S and polysulfide [38,39,45]. For the comparison, the potentials of peaks during the redox reactions of GNSCS/S and NSBPC/S were summarized in Fig. 5c. It is clearly observed that the GNSCS/S electrode has lower oxidation potential and higher reduction potential than NSBPC/S, suggesting that the GNSCS/S offers significantly lower polarization. It could be caused by the graphene-like carbon nanosheets which can expose a higher concentration of N/S-involved active sites for the oxidation/reduction of S/Li_2S. The result can be further testified by the charge/discharge voltage profiles of GNSCS/S and NSBPC/S electrodes in Fig. 5d at a current density of 0.3 A g^{-1} within a voltage window between 1.7 and 2.8 V *versus* Li^+/Li. A relatively small potential gap is clearly observed for GNSCS/S (~228 mV) than that of NSBPC/S (~331 mV) between charge and discharge curves. The lower polarization suggests the better electrochemical reaction dynamics and reversibility in the Li-S battery [46,47].

The rate performance of GNSCS/S and NSBPC/S electrodes was tested at different current densities (Fig. 6a). It can be clearly seen that the GNSCS/S delivers

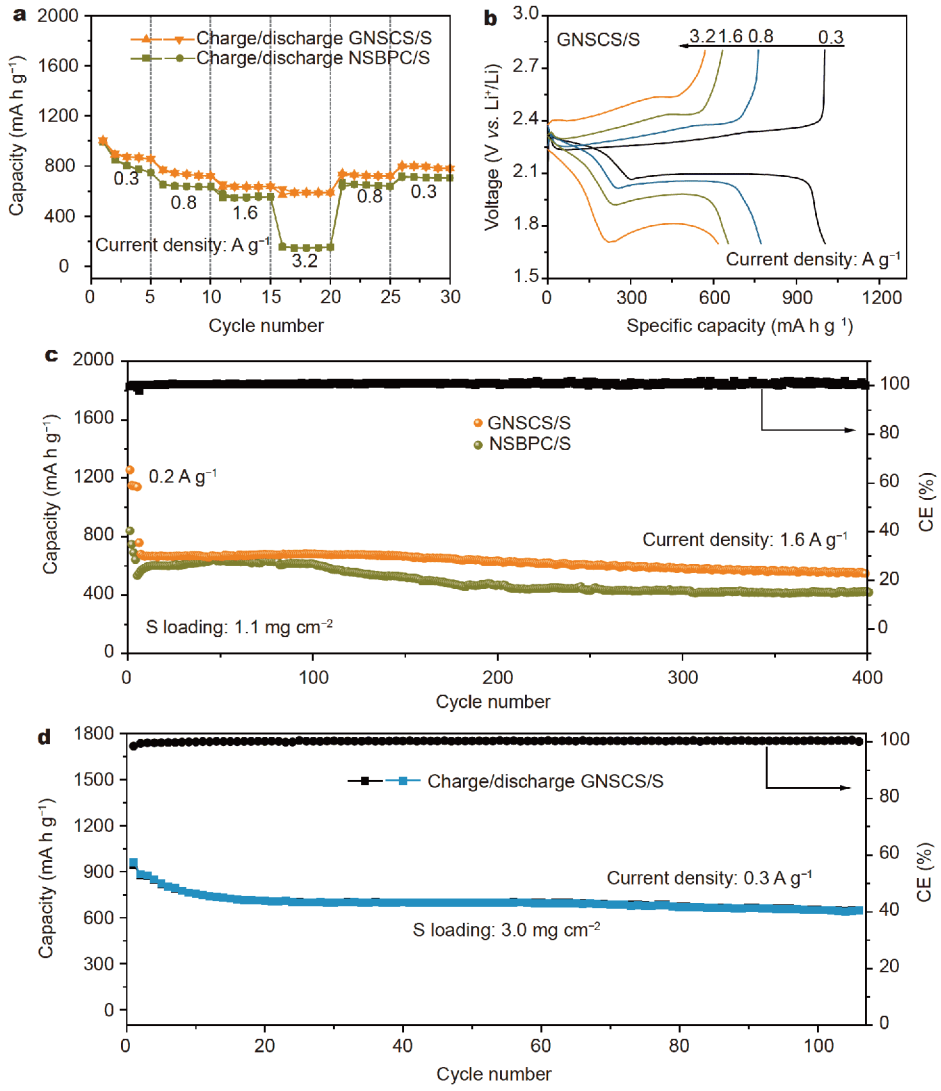

Figure 6 (a) Rate capability of GNSCS/S and NSBPC/S hybrids at different current rates, (b) discharge–charge voltage profiles of GNSCS/S at different current rates, (c) cycling performance of GNSCS/S and NSBPC/S at the current density of 1.6 A g^{-1}, (d) cycling performances of GNSCS/S at the current density of 0.3 A g^{-1} with a high areal sulfur loading of 3.0 mg cm^{-2}.

an initial discharge capacity of 1,003 mA h g^{-1} at current density of 0.3 A g^{-1}, slightly higher than that of NSBPC/S electrode (995 mA h g^{-1}). When the current density increases from 0.3 to 0.8 and 1.6 A g^{-1}, the discharge capacity is 1,003, 772 and 653 mA h g^{-1}, respectively. It is noteworthy that when the current density reaches up to 3.2 A g^{-1}, the discharge capacity of GNSCS/S remains about 587 mA h g^{-1}, much higher than that of the NSBPC/S electrode (142 mA h g^{-1}). It results from the good electronic conductivity favoring the kinetics [36] and the capacity performance at higher rates [29]. In addition, when the current density returns to 0.3 A g^{-1}, the GNSCS/S exhibits a discharge capacity of 793 mA h g^{-1} higher than that of NSBPC/S electrode (707 mA h g^{-1}), indicating a good rate performance of the GNSCS/S composites. The discharge–charge voltage profiles of both cathodes at various current rates are provided in Fig. 6b and Fig. S3. The respective discharge and charge plateaus of GNSCS/S are much longer than that of NSBPC/S electrode due to electrode polarization. Moreover, the plateau at higher rate is obviously shorter than that at lower rate, suggesting that the slow redox reaction kinetics and serious polarization are the performance-limiting factor in the condition of high current density [47].

To further demonstrate the durability of GNSCS/S

composite cathode, the long-term cycle behavior of GNSCS/S and NSBPC/S was investigated at the current density of 1.6 A g^{-1} in Fig. 6c. The first five cycles were activated at 0.2 A g^{-1} and the initial discharge capacity can reach up to 1,140 mA h g^{-1}. After activation, the cell was continually tested at a current density of 1.6 A g^{-1}. After 400 cycles, the GNSCS/S hybrid electrode delivered a better discharge capacity of 548 mA h g^{-1} with a capacity fade rate of only 0.13% per cycle. The initial CE of GNSCS/S is 99.7%, remaining around 100% during the whole testing process and suggesting the excellent reversibility of GNSCS/S electrode in the electrochemical process. In addition, a large capacity loss was also observed initially. From the XRD, it can be seen that the sulfur was largely located on the surface of the carbon hosts as the crystal. During the first several cycles, the sulfur and discharge products would redistribute on the surface after repeated electrochemical reactions, wherein some lithium polysulfides were not anchored by the carbon scaffolds and escaped into the electrolyte. Hence, the corresponding capacity of the cell was decreased during the initial cycling. Nevertheless, the NSBPC/S hybrid only delivers an initial discharge capacity of 839 mA h g^{-1} and discharge capacity of 423 mA h g^{-1} after 400 cycles. It is further testified that GNSCS/S can improve the cycling stability and rate performance of sulfur cathode superior to NSBPC relying on the doping effect. Fig. S4 describes the galvanostatic charge-discharge curves of GNSCS/S and NSBPC/S for the 20th, 30th, 40th, 50th and 100th cycles in the voltage window of 1.7–2.8 V *vs.* Li^+/Li at the current density of 1.6 A g^{-1}. The larger voltage gap between discharge and charge profiles of NSBPC/S electrode infers the much more serious polarization occurring during the charge–discharge process.

Considering the practical application of Li-S batteries, the electrode with a high areal sulfur loading of 3.0 mg cm^{-2} has been designed. Fig. 6d shows the corresponding cycle performance at a current density of 0.3 A g^{-1}. The discharge capacity can be initiated at 942 mA h g^{-1} and maintained at 647 mA h g^{-1} after more than 100 cycles with a high initial CE of 98.4%. The corresponding capacity fades only ~0.30% per cycle, demonstrating that the GNSCS/S hybrid still has excellent cycle stability and kinetics even as the sulfur loading was up to 3 mg cm^{-2}.

To dig out the excellence of GNSCS/S in Li-S batteries, galvanostatic intermittent titration technique (GITT) and EIS were used to explore the microstructure transition and the reaction kinetics in the electrochemical process [48,49]. The GITT curve is presented in Fig. 7a wherein

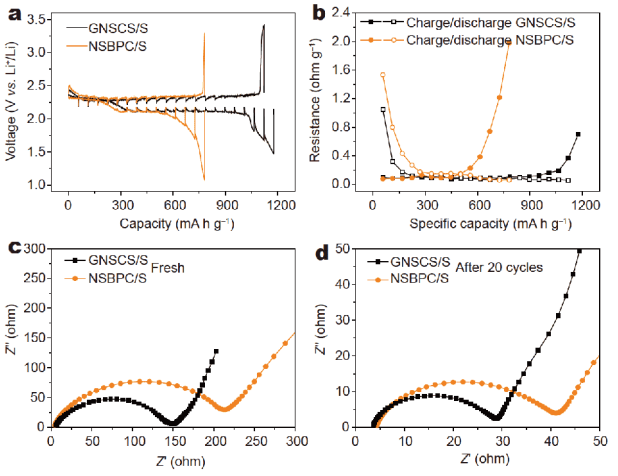

Figure 7 (a) GITT voltage and (b) reaction resistance profiles of GNSCS/S and NSBPC/S electrodes during the first charge/discharge cycle. The Nyquist plots of the two electrodes at the open-circuit voltage (c) and charged to 2.8 V after 20 cycles (d) with a frequency range of 100 kHz to 0.01 Hz at voltage amplitude of 10 mV.

GNSCS/S and NSBPC/S electrodes were charged/discharged by a series of current pulses at 0.1 C with an equal duration period of 20 min and followed by an equal interval time of 2 h. The plots of reaction resistance *vs.* specific capacity are derived for both samples during the GITT testing in Fig. 7b. The reaction resistance at the Li ion insertion/extraction process was calculated *via* dividing the overpotential (ΔE) by the pulse current density. As can be observed, the GNSCS/S electrode exhibits a higher capacity of 1,177.6 mA h g^{-1} than that of NSBPC/S electrode (1,121 mA h g^{-1}). During discharge progress, the reaction resistances for GNSCS/S and NSBPC/S electrodes dramatically decrease and then remain stable. What's more, the GNSCS/S electrode shows a lower reaction resistance than that of the NSBPC/S sample in the charge/discharge platforms. It can be inferred that the GNSCS/S electrode can enhance Li-ion insertion/extraction kinetics than that of the NSBPC/S sample.

The Nyquist plots of the two cell systems at the open-circuit voltage and after 20 cycles in the frequency range of 10^5–0.01 Hz at 10 mV amplitude are shown in Fig. 7c, d. A depressed semicircle in the high frequency region corresponds to the charge-transfer resistance (R_{ct}) occurring at the electrolyte–electrode interface. The sloped line in the low-frequency region accounts for the ion-diffusion process corresponding to the semi-infinite Warburg impedance [47,50]. Before discharging, the R_{ct} of GNSCS/S electrode is 144.1 Ω, much lower than that of NSBPC/S electrode (207.5 Ω). After charging/discharging

for 20 cycles, the R_{ct} of both electrodes largely decreases benefited by the activation process where the sulfur and Li_2S redistribute within the whole electrode [51]. However, the GNSCS/S electrode is still much smaller than NSBPC/S in R_{ct} value. This analytical result further confirms the acceleration of electronic and ion transportation and the improvement of the electrochemical activity by the heteroatom doping and the structure of graphene-like carbon nanosheets. In addition, the electrochemical performance of GNSCS/S electrode was compared in Table S1 with many other porous carbon derived from biomass used as sulfur holders in the literature [18,52–59].

CONCLUSIONS

In summary, graphene-like N/S-codoped bio-carbon nanosheets (GNSCS) were firstly fabricated by a facile and environment-friendly route. With the biomass as the raw sources, NaCl non-aqueous ionic liquid served as the exfoliation reagent to render the formation of graphene-like nanosheets. Furthermore, the electric conductivity of GNSCS is also greatly improved compared with that of bulk bio-carbon, favoring high-rate kinetics. When used as the cathode for Li-S batteries, it exhibits excellent cycling stability and rate capability and delivers a better discharge capacity of 548 mA h g^{-1} with a capacity fade rate of only 0.13% per cycle at a current density of 1.6 A g^{-1} after 400 cycles. The initial CE of GNSCS/S is as high as 99.7%. Even when the sulfur loading was up to 3 mg cm^{-2}, the discharge capacity can be maintained at 647 mA h g^{-1} after more than 100 cycles with a high initial CE of 98.4% and a low capacity degradation of only ~0.30% per cycle. The excellent electrochemical kinetics is largely resulting from N/S dual-doping and the graphene-like structure, favorably accelerating electron/ion transportation and providing sufficient active sites for chemically adsorbing polysulfides. This work paves the avenue for design and preparation of porous carbon materials from biomass with the aid of NaCl non-aqueous ionic liquid.

Received 18 June 2018; accepted 31 July 2018; published online 6 September 2018

1 Dunn B, Kamath H, Tarascon JM. Electrical energy storage for the grid: a battery of choices. Science, 2011, 334: 928–935
2 Manthiram A, Chung SH, Zu C. Lithium-sulfur batteries: progress and prospects. Adv Mater, 2015, 27: 1980–2006
3 Evers S, Nazar LF. New approaches for high energy density lithium–sulfur battery cathodes. Acc Chem Res, 2012, 46: 1135–1143
4 He J, Chen Y, Manthiram A. MOF-derived cobalt sulfide grown on 3D graphene foam as an efficient sulfur host for long-life lithium-sulfur batteries. iScience, 2018, 4: 36–43
5 He J, Chen Y, Manthiram A. Vertical Co_9S_8 hollow nanowall arrays grown on a Celgard separator as a multifunctional polysulfide barrier for high-performance Li–S batteries. Energy Environ Sci, 2018, doi:10.1039/C8EE00893K
6 Wei Seh Z, Li W, Cha JJ, *et al.* Sulphur–TiO_2 yolk–shell nanoarchitecture with internal void space for long-cycle lithium–sulphur batteries. Nat Commun, 2013, 4: 1331–1337
7 Zhang C, Lv W, Zhang W, *et al.* Reduction of graphene oxide by hydrogen sulfide: a promising strategy for pollutant control and as an electrode for Li-S batteries. Adv Energy Mater, 2014, 4: 1301565
8 Lv W, Li Z, Zhou G, *et al.* Tailoring microstructure of graphene-based membrane by controlled removal of trapped water inspired by the phase diagram. Adv Funct Mater, 2014, 24: 3456–3463
9 Wang L, Zhao Y, Thomas ML, *et al. In situ* synthesis of bipyramidal sulfur with 3D carbon nanotube framework for lithium-sulfur batteries. Adv Funct Mater, 2014, 24: 2248–2252
10 Miao L, Wang W, Yuan K, *et al.* A lithium–sulfur cathode with high sulfur loading and high capacity per area: a binder-free carbon fiber cloth–sulfur material. Chem Commun, 2014, 50: 13231–13234
11 Mi K, Jiang Y, Feng J, *et al.* Hierarchical carbon nanotubes with a thick microporous wall and inner channel as efficient scaffolds for lithium-sulfur batteries. Adv Funct Mater, 2016, 26: 1571–1579
12 Mi K, Chen S, Xi B, *et al.* Sole chemical confinement of polysulfides on nonporous nitrogen/oxygen dual-doped carbon at the kilogram scale for lithium-sulfur batteries. Adv Funct Mater, 2017, 27: 1604265
13 Zhang C, Wu HB, Yuan C, *et al.* Confining sulfur in double-shelled hollow carbon spheres for lithium-sulfur batteries. Angew Chem, 2012, 124: 9730–9733
14 Jayaprakash N, Shen J, Moganty SS, *et al.* Porous hollow carbon@sulfur composites for high-power lithium-sulfur batteries. Angew Chem, 2011, 123: 6026–6030
15 Zhao XS, Su F, Yan Q, *et al.* Templating methods for preparation of porous structures. J Mater Chem, 2006, 16: 637–648
16 He J, Lv W, Chen Y, *et al.* Direct impregnation of SeS_2 into a MOF-derived 3D nanoporous Co–N–C architecture towards superior rechargeable lithium batteries. J Mater Chem A, 2018, 6: 10466–10473
17 Imtiaz S, Zhang J, Zafar ZA, *et al.* Biomass-derived nanostructured porous carbons for lithium-sulfur batteries. Sci China Mater, 2016, 59: 389–407
18 Li J, Qin F, Zhang L, *et al.* Mesoporous carbon from biomass: one-pot synthesis and application for Li–S batteries. J Mater Chem A, 2014, 2: 13916–13922
19 Gu X, Wang Y, Lai C, *et al.* Microporous bamboo biochar for lithium-sulfur batteries. Nano Res, 2015, 8: 129–139
20 Yu M, Li R, Tong Y, *et al.* A graphene wrapped hair-derived carbon/sulfur composite for lithium–sulfur batteries. J Mater Chem A, 2015, 3: 9609–9615
21 Dupont J. From molten salts to ionic liquids: A "nano" journey. Acc Chem Res, 2011, 44: 1223–1231
22 Zhang J, Qiu Y, Huang M, *et al.* Accelerated formation of strontium silicate by solid-state reaction in NaCl–H_2O(v) system at lower temperature. Appl Surf Sci, 2015, 347: 57–63
23 Zhang J, Huang M, Yanagisawa K, *et al.* NaCl–H_2O-assisted preparation of $SrTiO_3$ nanoparticles by solid state reaction at low temperature. Ceramics Int, 2015, 41: 5439–5444
24 Liu F, Peng H, You C, *et al.* High-performance doped carbon

catalyst derived from Nori biomass with melamine promoter. Electrochim Acta, 2014, 138: 353–359
25 Ferrari AC, Meyer JC, Scardaci V, *et al.* Raman spectrum of graphene and graphene layers. Phys Rev Lett, 2006, 97: 187401
26 Ferrari AC, Basko DM. Raman spectroscopy as a versatile tool for studying the properties of graphene. Nat Nanotechnol, 2013, 8: 235–246
27 Ren W, Saito R, Gao L, *et al.* Edge phonon state of mono- and few-layer graphene nanoribbons observed by surface and interference co-enhanced Raman spectroscopy. Phys Rev B, 2010, 81: 035412
28 Sangwichien C, Aranovich GL, Donohue MD. Density functional theory predictions of adsorption isotherms with hysteresis loops. Colloids Surfs A-Physicochem Eng Aspects, 2002, 206: 313–320
29 Fang R, Zhao S, Pei S, *et al.* Toward more reliable lithium–sulfur batteries: an all-graphene cathode structure. ACS Nano, 2017, 10: 8676–8682
30 Zhang Z, Li Z, Hao F, *et al.* 3D interconnected porous carbon aerogels as sulfur immobilizers for sulfur impregnation for lithium-sulfur batteries with high rate capability and cycling stability. Adv Funct Mater, 2014, 24: 2500–2509
31 Li GC, Li GR, Ye SH, *et al.* A polyaniline-coated sulfur/carbon composite with an enhanced high-rate capability as a cathode material for lithium/sulfur batteries. Adv Energy Mater, 2012, 2: 1238–1245
32 Sun D, Yang J, Yan X. Hierarchically porous and nitrogen, sulfur-codoped graphene-like microspheres as a high capacity anode for lithium ion batteries. Chem Commun, 2015, 51: 2134–2137
33 Yang J, Ju Z, Jiang Y, *et al.* Enhanced capacity and rate capability of nitrogen/oxygen dual-doped hard carbon in capacitive potassium-ion storage. Adv Mater, 2018, 30: 1700104
34 Kiciński W, Szala M, Bystrzejewski M. Sulfur-doped porous carbons: Synthesis and applications. Carbon, 2014, 68: 1–32
35 Gu W, Sevilla M, Magasinski A, *et al.* Sulfur-containing activated carbons with greatly reduced content of bottle neck pores for double-layer capacitors: a case study for pseudocapacitance detection. Energy Environ Sci, 2013, 6: 2465–2476
36 Pang Q, Tang J, Huang H, *et al.* A nitrogen and sulfur dual-doped carbon derived from polyrhodanine@cellulose for advanced lithium-sulfur batteries. Adv Mater, 2015, 27: 6021–6028
37 Hou TZ, Chen X, Peng HJ, *et al.* Design principles for heteroatom-doped nanocarbon to achieve strong anchoring of polysulfides for lithium-sulfur batteries. Small, 2016, 12: 3283–3291
38 Qiu Y, Li W, Zhao W, *et al.* High-rate, ultralong cycle-life lithium/sulfur batteries enabled by nitrogen-doped graphene. Nano Lett, 2014, 14: 4821–4827
39 Wang X, Weng Q, Liu X, *et al.* Atomistic origins of high rate capability and capacity of N-doped graphene for lithium storage. Nano Lett, 2014, 14: 1164–1171
40 Sun F, Wang J, Chen H, *et al.* High efficiency immobilization of sulfur on nitrogen-enriched mesoporous carbons for Li–S batteries. ACS Appl Mater Interfaces, 2013, 5: 5630–5638
41 Song J, Xu T, Gordin ML, *et al.* Nitrogen-doped mesoporous carbon promoted chemical adsorption of sulfur and fabrication of high-areal-capacity sulfur cathode with exceptional cycling stability for lithium-sulfur batteries. Adv Funct Mater, 2014, 24: 1243–1250
42 Zhou G, Paek E, Hwang GS, *et al.* Long-life Li/polysulphide batteries with high sulphur loading enabled by lightweight three-dimensional nitrogen/sulphur-codoped graphene sponge. Nat Commun, 2015, 6: 7760–7771
43 Guo J, Xu Y, Wang C. Sulfur-impregnated disordered carbon nanotubes cathode for lithium–sulfur batteries. Nano Lett, 2011, 11: 4288–4294
44 Zhang FF, Huang G, Wang XX, *et al.* Sulfur-impregnated core-shell hierarchical porous carbon for lithium-sulfur batteries. Chem Eur J, 2014, 20: 17523–17529
45 Fang R, Zhao S, Sun Z, *et al.* More reliable lithium-sulfur batteries: status, solutions and prospects. Adv Mater, 2017, 29: 1606823
46 Zheng G, Yang Y, Cha JJ, *et al.* Hollow carbon nanofiber-encapsulated sulfur cathodes for high specific capacity rechargeable lithium batteries. Nano Lett, 2011, 11: 4462–4467
47 Li L, Chen L, Mukherjee S, *et al.* Phosphorene as a polysulfide immobilizer and catalyst in high-performance lithium-sulfur batteries. Adv Mater, 2017, 29: 1602734
48 Zhao J, Zou X, Zhu Y, *et al.* Electrochemical intercalation of potassium into graphite. Adv Funct Mater, 2016, 26: 8103–8110
49 Zhou G, Pei S, Li L, *et al.* A graphene-pure-sulfur sandwich structure for ultrafast, long-life lithium-sulfur batteries. Adv Mater, 2014, 26: 625–631
50 Li L, Wu ZP, Sun H, *et al.* A foldable lithium–sulfur battery. ACS Nano, 2015, 9: 11342–11350
51 Han J, Xi B, Feng Z, *et al.* Sulfur–hydrazine hydrate-based chemical synthesis of sulfur@graphene composite for lithium–sulfur batteries. Inorg Chem Front, 2018, 5: 785–792
52 Yang K, Gao Q, Tan Y, *et al.* Microporous carbon derived from Apricot shell as cathode material for lithium–sulfur battery. Microporous Mesoporous Mater, 2015, 204: 235–241
53 Zhang S, Zheng M, Lin Z, *et al.* Activated carbon with ultrahigh specific surface area synthesized from natural plant material for lithium–sulfur batteries. J Mater Chem A, 2014, 2: 15889–15896
54 Wei S, Zhang H, Huang Y, *et al.* Pig bone derived hierarchical porous carbon and its enhanced cycling performance of lithium–sulfur batteries. Energy Environ Sci, 2011, 4: 736–740
55 Park MS, Yu JS, Kim KJ, *et al.* Porous carbon spheres as a functional conducting framework for use in lithium–sulfur batteries. RSC Adv, 2013, 3: 11774–11781
56 Zhang B, Xiao M, Wang S, *et al.* Novel hierarchically porous carbon materials obtained from natural biopolymer as host matrixes for lithium–sulfur battery applications. ACS Appl Mater Interfaces, 2014, 6: 13174–13182
57 Wang H, Chen Z, Liu HK, *et al.* A facile synthesis approach to micro–macroporous carbon from cotton and its application in the lithium–sulfur battery. RSC Adv, 2014, 4: 65074–65080
58 Xin S, Gu L, Zhao NH, *et al.* Smaller sulfur molecules promise better lithium–sulfur batteries. J Am Chem Soc, 2012, 134: 18510–18513
59 Zhao S, Li C, Wang W, *et al.* A novel porous nanocomposite of sulfur/carbon obtained from fish scales for lithium–sulfur batteries. J Mater Chem A, 2013, 1: 3334–3339

Acknowledgements The authors gratefully acknowledge the financial supports provided by the National Natural Science Foundation of China (21601108 and U1764258), Young Scholars Program of Shandong University (2017WLJH15), the Fundamental Research Funds of Shandong University (2016JC033 and 2016GN010), and the Taishan Scholar Project of Shandong Province (ts201511004).

Author contributions Xiong S and Huang M conceived the idea. Huang M and Xi B planned and performed the experiments, collected and analyzed the data. Huang M and Xiong S co-wrote the manuscript. All authors discussed the results and commented on the manuscript.

Conflict of interest The authors declare no conflict of interest.

Supplementary information Supporting data are available in the online version of the paper.

Man Huang got her Master degree from Jiangsu University of Science and Technology. Now, she is a PhD student under the supervision of Prof. Shenglin Xiong and Prof. Yitai Qian at the School of Chemistry and Chemical Engineering, Shandong University, China. Her research interests mainly focus on the design and fabrication of novel carbon nanostructures for energy conversion and storage.

Shenglin Xiong received his PhD degree in inorganic chemistry from the University of Science & Technology of China in 2007. He worked at National University of Singapore from 2009 to 2011 as a Research Fellow. He is now a professor at the School of Chemistry and Chemical Engineering, Shandong University. His research interests include the design and development of micro/nanostructured composite materials and their applications in energy storage and conversion.

在NaCl非水离子液体中制备类石墨烯状氮硫共掺杂生物质碳材料来提高锂硫电池的动力学研究

黄曼[1], 杨靖宇[1], 奚宝娟[1], 弭侃[1], 封振宇[1], 刘静[2], 冯金奎[3], 钱逸泰[1,4], 熊胜林[1*]

摘要 本论文通过结构设计利用简单方法成功制备了一种二维N,S共掺杂类石墨烯纳米片复合结构, 即利用NaCl非水离子液体的剥离作用使生物质剥离得到二维片层类石墨烯结构. 这种新的非水离子液体剥离技术较其他的碳材料剥离技术具有环境友好性、低成本、安全无毒性等优势, 有利于实现量化制备锂硫电池电极材料. 该材料采用大自然中广泛存在的紫菜作为原料, 其内部富含的氨基酸为原位掺杂N,S元素提供了可能性. 二维结构的纳米片能够提供有效的导电性和电解液浸润性的网络结构, 同时还能够有效地降低电池在充放电循环过程中导致的体积膨胀效应, 最终实现一种高机械性能、优异电化学活性的电极在锂硫电池储能领域中的应用.

